ASTFE
American Society
of Thermal and Fluids Engineers

5th Thermal and Fluids Engineering Conference (TFEC)
April 5–8, 2020
New Orleans, LA, USA

TFEC-2020-31960

Examination of compressibility effects in the Falkner-Skan equations

Miguel A. Ramírez, Guillermo Araya*

High Performance Computing and Visualization Laboratory (HPCVL), Department of Mechanical Engineering, University of Puerto Rico, Mayaguez, PR 00681, USA

ABSTRACT

The Navier-Stokes (NS) equations are the cornerstone of fluid mechanics. It is solved for given initial and boundary conditions in order to study the dynamics of fluids. Falkner-Skan (FS) developed a solution for these equations in laminar flow, as a generalization of the Blasius boundary layer. The idea is to represent accelerating (Favorable Pressure Gradient, FPG) or decelerating (Adverse Pressure Gradient, APG) flows, whose freestream velocity varies as a power law of the streamwise coordinate. the primary purpose of this work is to solve this set of equations for the laminar compressible flow case subject to streamwise pressure gradients via the use of the Illingworth (which considers only the effects of the local density) and Howarth (which takes into account the changes of the local density with respect to the free stream density) transformations, by considering supersonic and hypersonic Mach numbers and different wall temperature conditions (cold, adiabatic and hot wall conditions). It will also include a study of different pressure gradient parameters (i.e., β parameter). In conclusion, the algorithm developed for Falkner-Skan incompressible and compressible flow was effectively validated. As the Mach number increases up to hypersonic levels, the temperature ratio significantly increases in the near wall region for adiabatic conditions. It is important to mention that as the Mach number increases, the velocity boundary layer thickness decreases, whereas the shear stress near the wall increases.

KEY WORDS: Falkner-Skan, Compressible Flow, Laminar, Turbulence, Skin friction, Boundary Layer

1. INTRODUCTION AND THEORETICAL BACKGROUND

New technologies always require new tactics for their understanding. As technology progresses the speed of the fluid flow increases and the problems that come with it become more apparent (large variations in density with respect to pressure). Therefore, new methods and studies are required to solve these issues. One important aspect to start solving this problem is the fluid motion characterization via the Navier-Stokes equations for compressible flow in aerodynamic high-speeds.

The Navier-Stokes (NS) equations are the cornerstone of fluid mechanics. The Clay Mathematics Institute [1] has called the analytical solution in three-dimensions of NS equations as one of the seven most important open problems in mathematics. Numerically, they are solved for given initial and boundary conditions in order to study the fluid dynamics. There are few analytical or semi-analytical solutions for these equations due to its complexity, non-linearity and three-dimensionality. According to the Prandtl theory [2, 3] these equations can be solved by dividing the flow in two regions separated by a boundary layer. As seen in Figure 1 these regions are classified as a near wall region or boundary layer where the viscosity effects are important, and a further wall region were the viscosity effect are practically negligible (inviscid flow).

*Corresponding Author: araya@mailaps.org

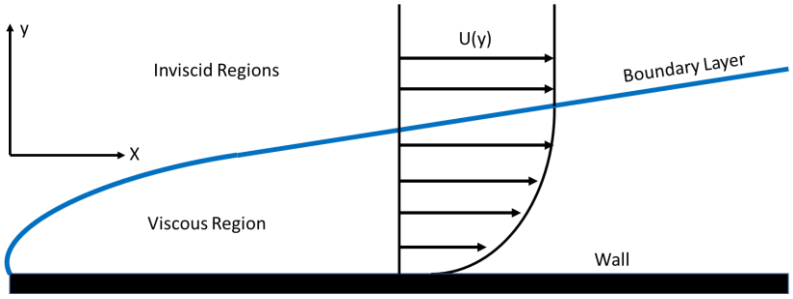

Fig. 1: Prandtl Boundary Layer Diagram.

With the help of Prandtl theory, Blasius [4] developed a general solution of the Navier-Stokes equations by introducing the concept of similarity to the NS equations and solving them for a flat plate. Later, Falkner and Skan [4] introduced the streamwise pressure gradient concept to give a more general solution for wedges and constant pressure gradient situations. At the end, the final equations obtained from this analysis can be used to obtain the boundary layer thickness, the skin friction coefficient, the local streamwise and wall-normal velocity components, etc. via a Runge-Kutta or numerical integration.

As previously stated, as technology and high-speed vehicles progress the fluid free stream velocity significantly increases until the flow becomes compressible and the thermodynamic effects needed to be accounted for in the Falkner-Skan equations. It is important to mention that compressibility effects are very difficult to study, because of its high-density variation with pressure, particularly in hypersonic flows, i.e. for Mach numbers larger than or equal to 5.

A few years later, Horwath and Illingworth proposed a solution to the FS equations for compressible flows by taking in to account the changes in density and coupling them with the energy equation. Howarth [4] solution reduces the compressible boundary layer to an incompressible boundary layer by assuming a constant free stream velocity and Illingworth [5] solution calculates the effect of compressibility on the separation of the laminar boundary layer by assuming a linearly retarded mainstream which yield more accurate results than Howarth [6]. With any of these two approaches the FS equations can be solved for compressible to obtain the parameters mentioned above.

The original Falkner-Skan equations assume laminar flow. However, most of the wall-bounded flows are turbulent, which the flow is chaotic and not very easy to study. Thus, most flows studied in fluid mechanics is dominated by compressibility effects and turbulence effects. Turbulence is characterized by a huge range between length and time scales, flow fluctuations and large Reynolds numbers. The main difference between turbulent and laminar boundary layers is that in the laminar section mass, momentum and energy are transported among streamlines in an orderly manner by molecular diffusion, but turbulent is characterized by disorderly and rapid fluctuations called eddies which transport the energy, momentum and mass mush rapidly than molecular diffusion greatly enhancing them. As a consequence, the equation to study the laminar flow are obtained analytically but for turbulence flow, due to the fact that that eddies are not so easy to study, turbulent flow is studied with semiempirical equations [2, 7]. The main approach to study turbulent flow is via the law of the wall. This law is a dimensional analysis of the near wall region assuming that the turbulence near the boundary is a function of the flow conditions at that wall and independent of flow conditions further away [8]. Other parameters studied are the Reynolds turbulence intensities which gives an idea of the magnitude of the turbulence fluctuations and the Reynolds stresses which are proportional to the forces on the fluid due to turbulence nature. An important aspect is that if compressible flow is considered a temperature boundary layer develops and must be considered in the analysis.

Research has been done to study the boundary layer turbulent flow. Xenos, *et al*. [9] studied the compressible turbulent boundary-layer flow over a permeable wedge numerically and its effects of localized suction, applied to the region of the separation point. The compressible turbulent boundary-layer flow was studied via the models of Cebeci–Smith (C–S) and Baldwin–Lomax (B–L). They concluded that as the power parameter m increased, the dimensionless skin friction coefficient C_f, the local Stanton number S_t, and the total drag D, increase as well. Suction always increases the total drag over the wedge; and injection decreases the total drag over the wedge. Also, they stated that the combination of the localized suction and injection is important for drag reduction and prevention of boundary-layer separation. Furthermore, in Xenos and Pop [10], it was studied the effects of thermal radiation and localized suction on the steady turbulent compressible boundary

layer flow with adverse pressure gradient. Thermal radiation has significant effects on the flow field, especially at high temperatures. Two algebraic turbulence models: the Cebeci and Smith (C–S) [11] the Baldwin Lomax (B–L) [12]. They found that the thermal radiation and localized suction influenced all the important flow characteristics (separation point, total drag, and the thermal boundary layer) and that the effect of radiation altered the thermal boundary layer above the flat plate giving it a cooling effect on the fluid at the plate vicinity and a slight increase of the maximum temperature of the compressible boundary layer. Knight *et al*. [13]. developed a Large Eddy Simulation (LES) approach for an expanding corner flow at Mach 3 and validated it with experiments, obtaining very good agreement as seen in their Figures 3 and 4.

Holden *et al*. [14] conducted an experiment to examine the changes in the structure at the base of a hypersonic turbulent boundary layer subjected to a strong self-induced pressure gradient in regions of shock wave/boundary layer interaction and obtained results in agreement with the law of the wall for the velocity distribution at Mach numbers of 11, 13 and 16 (see figures 5 and 6 in [14]).

Xu and Martin [15] proposed an inflow generation methodology, inspired by the strong Reynolds analogy (SRA), for compressible turbulent boundary layers. They showed good agreement with the Walz equation distribution.

In addition, there have been a wide range of aircraft and other vehicles in which supersonic and hypersonic flow theory have been applied. One of the first was the Silbervogel orbital bomber in which Sanger and Bredt [16] tried to solve and state the problems and solutions of supersonic flight at Mach 3. Another, application is in hypersonic missiles. These missiles travel almost at Mach 6 and they are highly manoeuvrable which makes them very difficult to intercept and destroy [17]. Also, according to NASA hypersonic and supersonic flow have a very important impact in space shuttle re-entry due to the high Mach numbers achieve (around Mach 10) [18].

This work is an attempt to solve the Falkner-Skan equations for compressible flow via the Illingworth and Horwath transformations [19]. By comparing the obtained results with incompressible flow solutions, the corresponding compressibility effects will be evaluated.

2. MATHEMATICAL ANALISIS

This section shows the mathematical analysis used to obtain the solution of the FS equations for laminar incompressible and compressible flows, as well as an alternate solution to the compressible flow.

2.1 The Compressible Navier Stokes Equations

The Navier –Stokes Equations are divided in three sections: a continuity equation which takes into account the continuity of the flow, a momentum equation which studies the dynamic of the flow and energy equation which studies the fluid energy movement.

The continuity equation is given as:

$$\frac{\partial \rho}{\partial t} + \frac{\partial}{\partial x}(\rho u) + \frac{\partial}{\partial y}(\rho v) = 0 \tag{1}$$

The x momentum equation is given as:

$$\rho\left(\frac{\partial u}{\partial t} + u\frac{\partial u}{\partial x} + v\frac{\partial u}{\partial y}\right) = -\frac{\partial \rho_e}{\partial x} + \frac{\partial}{\partial y}\left(\mu\frac{\partial u}{\partial y}\right) \tag{2}$$

The y momentum equation is given as:

$$\frac{\partial p}{\partial y} = 0 \tag{3}$$

The energy equation is given as:

$$\rho\left(\frac{\partial h}{\partial t}+u\frac{\partial h}{\partial x}+v\frac{\partial h}{\partial y}\right)=\frac{\partial p_e}{\partial t}+u\frac{\partial p_e}{\partial x}+\frac{\partial}{\partial y}\left(k\frac{\partial T}{\partial y}\right)+\mu(\frac{\partial u}{\partial y})^2 \quad (4)$$

2.2 The Incompressible Navier Stokes Equations

In the steady incompressible flow, if buoyancy is neglected the velocity is uncoupled from the temperature field. This means that the Navier-Stokes equations can be applied without taking in to account the energy section [4]. Applying this assumption to equation 1 and 2, the Navier-Stokes equation becomes:

The continuity equation:

$$\frac{\partial u}{\partial x}+\frac{\partial v}{\partial y}=0 \quad (5)$$

The *x*-momentum equation in two-dimensional form reads:

$$\left(u\frac{\partial u}{\partial x}+v\frac{\partial u}{\partial y}\right)=U\frac{dU}{dx}+\mu\frac{\partial^2 u}{\partial y^2} \quad (6)$$

2.3 The Falkner Skan Compressible Flow Solution

The Falkner-Skan solution for compressible flow is obtained via the application of the Illinworth and the Howarth transformation to the NS equations (equations 1, 2, 3, 4).

Illingworth accounted for viscosity effects in ξ and η, as seen in the following equations [19]:

$$\xi=\int_0^x \rho_e(x)\,U_e(x)\,\mu_e(x)\,dx \quad (7)$$

$$\eta=\frac{U_e}{\sqrt{2\xi}}\int_0^y \rho\,dy \quad (8)$$

Howarth considered the variation of the ratio between the freestream density and the local density [20]:

$$\eta=Y_1\sqrt{\frac{U}{2v_\infty x_1}} \quad (9)$$

$$Y_1=\int_0^Y \frac{\rho}{\rho_\infty}\,dY \quad (10)$$

$$x_1=x \quad (11)$$

Applying this similarity equations (Illingworth or Horwath) to the NS compressible equations (equations 1, 2, 3, 4) the following Falkner-Skan compressible flow equations are obtained:

Momentum equation:

$$C*F'''+FF''=\beta*(F'*F'-g) \quad (12)$$

Energy equation:

$$C*g''+Pr*F*g'=-B*C*(F''*F'') \quad (13)$$

Where:

$$C = g^{-1/3} \tag{14}$$

$$B = Pr * (\gamma - 1) * M_{ae}^2 \tag{15}$$

In this equations *F*'' is related to the shear stress, *F*' is related to the velocity, *F* is related to the stream function, β is the pressure gradient related to the wedge angle, *C* is the ratio between the density and viscosity and the stream density and viscosity, *g*' is related to the thermal gradient and *g* is related to the temperature and density ratios.

The local velocity can be obtained as:

$$u = U_e F' \tag{16}$$

The skin friction coefficient is obtained as:

$$C_f = \frac{2\tau_w}{\rho_e U_e^2} \tag{17}$$

The β parameter can be obtained as:

$$\beta = 2 * \theta / \pi \tag{18}$$

The boundary layer can be obtained by finding η where the local speed is 99% of the freestream velocity, this value is used in equation 6 to obtain the *y* coordinate when this happens for different *x* values. Note that the Blasius solution can be obtained by setting *C* = 1 and β = 0 for a flat plate.

2.4 The Falkner Skan Alternate Compressible Flow Solution

As stated in section 2.3, the alternate Falkner-Skan solution for compressible flow is obtained via the application of the Illinworth (equation 7 and 8) and the Howarth (equation 9, 10 and 11) transformation to the NS equations (equations 1, 2, 3, 4).

Applying this similarity equations (Illingworth or Horwath) to the NS compressible equations (equations 1, 2, 3, 4) a more general Falkner-Skan compressible flow equations can be obtained by assuming $C = g^p$.

Momentum equation:

$$P * g^{(P-1)} * g' * F'' + g^P * F''' + F * F'' = \beta * (F' * F' - g) \tag{19}$$

Energy equation:

$$P * g^{(P-1)} * g' * g' + g^P * g'' + Pr * F * g' = -B * g^p * (F'' * F'') \tag{20}$$

Where:

$$P = -0.24 \tag{21}$$

$$B = Pr * (\gamma - 1) * M_{ae}^2 \tag{22}$$

As same in section 2.3, in this equations *F*'' is related to the shear stress, *F*' is related to the velocity, *F* is related to the stream function, β is the pressure gradient related to the wedge angle, *P* is the compressible Falkner Skan power, *g*' is related to the thermal gradient and *g* is related to the temperature and density ratios.

The local velocity, the skin friction coefficient and the pressure gradient parameter can be obtained by using equations 16, 17 and 18 located in section 2.3.

Note: The flat plate special case of C=1 can be obtained by setting P (equation 21) and β to zero.

2.5 The Falkner Skan Incompressible Flow Solution

The Falkner-Skan solution for incompressible flow is obtain via the application of a similarity transformation to the NS equations (equations 5 and 6).

Falkner Skan (1931) found that the similarity condition was achieved when:

$$\eta = C\ yx^a \tag{23}$$

Where:

$$U(x) = Kx^m \tag{24}$$

$$m = 2a + 1 \tag{25}$$

$$C^2 = \frac{K(1+m)}{2\Lambda} \tag{26}$$

Note: Λ is the kinematic viscosity in m^2/s.

Applying equations 24, 25 and 26 into equation 23 the similarity equation is obtained as:

$$\eta = Y\sqrt{\frac{(m+1)*U(x)}{2\Lambda x}} \tag{27}$$

Applying this similarity equation (equation 27) to the NS incompressible equations (equations 5 and 6) the following Falkner-Skan incompressible flow equations are obtained:

Momentum equation:

$$F''' + FF'' + \beta * (1 - F' * F') = 0 \tag{28}$$

In this equation, *F*'' is related to the shear stress, *F*' is related to the velocity, *F* is related to the stream function, β is the pressure gradient related to the wedge angle.

The local velocity can be obtained as:

$$u = U_e F' \tag{29}$$

The skin friction coefficient is obtained as:

$$C_f = \frac{2\tau_w}{\rho_e U_e^2} \tag{30}$$

The β parameter can be obtained as:

$$\beta = 2 * \theta/\pi \tag{31}$$

Or

$$\beta = \frac{2m}{1+m} \quad (32)$$

The boundary layer can be obtained by finding η where the local speed is 99% of the free stream velocity, this value is used in equation 23 to obtain the *y* coordinate when this happens for different *x* values. Note that the Blasius solution can be obtained by setting $\beta = 0$ for a flat plate.

3. NUMERICAL DETAILS

This section shows the analysis done to solve the Falkner Skan equations for laminar compressible, alternate compressible and incompressible flows solutions as well as its boundary conditions.

3.1 Falkner Skan Laminar Compressible Flow Solution

In order to solve the Falkner-Skan compressible equation, it needs to be transformed in to first order differential equation.

This is done as follows:

1) The following values are set up as:

$$Y_1 = F'' = \frac{d^2F}{d\eta} \quad (33)$$

$$Y_2 = F' = \frac{\partial F}{\partial \eta} \quad (34)$$

$$Y_3 = F \quad (35)$$

$$F''' = [\beta(F'F' - g) - FF'']/C \quad (36)$$

$$Y_4 = g' = \frac{dg}{d\eta} \quad (37)$$

$$Y_6 = g \quad (38)$$

$$g'' = (-B\ C\ (F"\ F") - \Pr(Fg'))/C \quad (39)$$

2) After solving the following differential equations, the following matrix is obtained:

$$\begin{bmatrix} Y_1^{n+1} \\ Y_2^{n+1} \\ Y_3^{n+1} \\ Y_4^{n+1} \\ Y_6^{n+1} \end{bmatrix} = \begin{bmatrix} Y_1^n + (\Delta n * (0.33 * (Y_2^n - Y_6^n) - Y_3^n * Y_1^n)/C^n) \\ Y_2^n + \Delta n * Y_1^n \\ Y_3^n + \Delta n * Y_2^n \\ Y_4^n - \Delta n * (Pr * Y_3^n * Y_4^n + B * C^n * (Y_1^n * Y_1^n))/C^n) \\ Y_6^n + \Delta n * Y_4^n \end{bmatrix} \quad (40)$$

Where Y^n is the previous values and Y^{n+1} are the forward values.

3.2 Falkner Skan Laminar Alternate Compressible Flow Solution

In order to solve the Falkner-Skan alternate compressible equation, it needs to be transformed in to first order differential equation.

This is done as follows:

1) The following values are set up as:

$$Y_1 = F'' = \frac{d^2F}{d\eta} \quad (41)$$

$$Y_2 = F' = \frac{\partial F}{\partial \eta} \quad (42)$$

$$Y_3 = F \quad (43)$$

$$F''' = \left[\beta(F'F' - g) - Pg^{(P-1)}g'^{F''} - FF''\right]/g^P \quad (44)$$

$$Y_4 = g' = \frac{dg}{d\eta} \quad (45)$$

$$Y_6 = g \quad (46)$$

$$g'' = (-B\ g^P\ (F''\ \mathrm{F}'') - \mathrm{P}g^{(P-1)}(g'g') - PrFg')/g^P \quad (47)$$

2) After solving the following differential equations, the following matrix is obtained:

$$\begin{bmatrix} Y_1^{n+1} \\ Y_2^{n+1} \\ Y_3^{n+1} \\ Y_4^{n+1} \\ Y_6^{n+1} \end{bmatrix} = \begin{bmatrix} Y_1^n + (\Delta n * (\beta * (Y_2^n * Y_2^n - Y_6^n) - PY_6{n^{P-1}} * Y_4^n * Y4_1^n - Y_3^n * Y_1^n)/Y_6{n^P}) \\ Y_2^n + \Delta n * Y_1^n \\ Y_3^n + \Delta n * Y_2^n \\ Y_4^n - \Delta n * (B * Y_6{n^P} * (Y_1^n * Y_1^n) + P * Y_6{n^{P-1}} * Y_4^n * Y_4^n + Pr * Y_3^n * Y_4^n)/Y_6{n^P}) \\ Y_6^n + \Delta n * Y_4^n \end{bmatrix} \quad (48)$$

Where Y^n is the previous values and Y^{n+1} are the forward values.

3.3 Falkner Skan Laminar Compressible and Alternate Compressible Flow Solutions Boundary Conditions

This type of problem is solved as an Initial Condition or Initial Boundary value problem. Figure 2 shows the setup of the laminar compressible flow simulation.

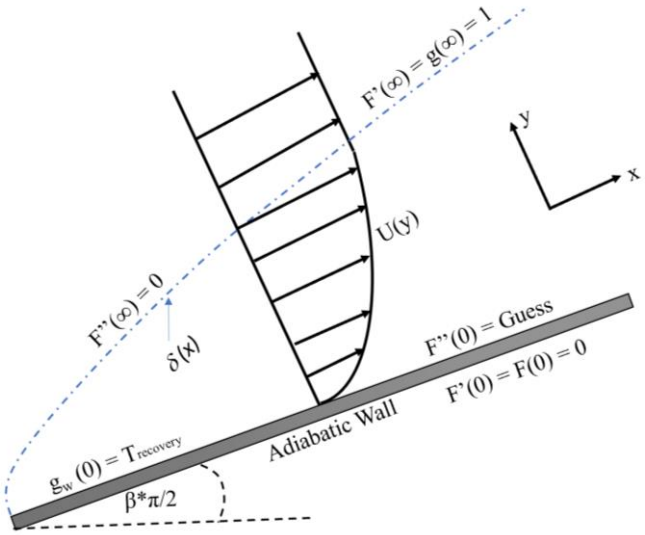

Fig. 2: Simulation set up diagram.

The initial boundary conditions near the wall are:

$$F'(0) = F(0) = 0 \quad (49)$$

$$g(0) = T_{adiabatic} = 1 + r * \frac{\gamma-1}{2} M_e^2 \quad (50)$$

$$g'(0) = 0 \; for \; Adiabatic \; wall \quad (51)$$

$$F''(0) = Guess \quad (52)$$

Where r is the recovery factor obtain as a function of the Prandtl number. The initial boundary conditions far from the wall:

$$F'(\infty) = 1 \tag{53}$$

$$g(\infty) = 1 \tag{54}$$

3.4 Falkner Skan Laminar Compressible Flow Simulation Algorithm

The Falkner-Skan compressible equations are solved by using the point and shoot method which can be solved via a numerical derivative or a Runge Kutta method. In this work a numerical derivative was used to solve this equation. Note that in the point and shoot method the value of *F*''(0) is guessed until the condition *F*'(∞) = 1 is achieved.

The algorithm is as follows:
Inputs: Mach, ρ, μ, Pr, r, γ, L_y, h_y, β
$\upsilon = \mu/\rho$
$B = Pr * (\gamma - 1) * M^2$
Form η vector
Initial conditions: Y1=Guess, Y2=0, Y3=0, Y4=0, Y6=g_w
Loop start: for (i=1; length vector)
Previous values storage: Y10=Y1, Y20=Y2, Y30=Y3, Y40=Y4, Y60=Y6, C=1
$Y1 = \left(\Delta\eta * \frac{\beta * Y20 * Y20 - Y30 * Y10}{C}\right) + Y10$
$Y2 = Y20 + \Delta\eta * Y10$
$Y3 = Y30 + \Delta\eta * Y20$
$Y4 = Y40 - \left(\Delta\eta * \frac{B * C * Y10 * Y10 + Pr * Y30 * Y40}{C}\right)$
$Y6 = Y60 + \Delta\eta * Y40$
Values storage (arrays): Y1(i)=Y1, Y2(i)=Y2, Y3(i)=Y3, Y4(i)=Y4, Y6(i)=Y6
Loop end

3.5 Falkner Skan Laminar Alternate Compressible Flow Simulation Algorithm

The Falkner-Skan alternate compressible equations are solved by using the point and shoot method which can be solved via a numerical derivative or a Runge Kutta method. In this work a numerical derivative was used to solve this equation.

Note: In the point and shoot method the value of *F*''(0) is guessed until the *F*'(∞) = 1 is reached.

The algorithm is as follows:
Inputs: Mach, ρ, μ, Pr, r, γ, L_y, h_y, β
$\upsilon = \mu/\rho$
$B = Pr * (\gamma - 1) * M^2$
Form eta vector
Initial conditions: Y1=Guess, Y2=0, Y3=0, Y4=0, Y6=gw
Loop Start: for (i=1; length vector)
Previous Values Storage: Y10=Y1, Y20=Y2, Y30=Y3, Y40=Y4, Y60=Y6, P=0 or -0.24
$Y1 = Y10 + \Delta\eta * (\beta * (Y20 * Y20 - Y60) - P * Y60^{P-1} * Y40 * Y10 - Y30 * Y10)/Y60^P$
$Y2 = Y20 + \Delta\eta * Y10$
$Y3 = Y30 + \Delta\eta * Y20$
$Y4 = Y40 - \Delta\eta * (B * Y60^P * Y10 * Y10 + P * Y60^{P-1} * Y40 * Y40 + Pr * Y30 * Y40)/Y60^P$
$Y6 = Y60 + \Delta\eta * Y40$
Values Storage (Arrays): Y1(i)=Y1, Y2(i)=Y2, Y3(i)=Y3, Y4(i)=Y4, Y6(i)=Y6
Loop end

3.6 Falkner Skan Laminar Incompressible Flow

The Falkner-Skan incompressible equation needs to be transformed in to first order differential equation, as follows:

1) The following values are set up as:

$$Y_1 = F'' = \frac{d^2F}{d\eta} \tag{55}$$

$$Y_2 = F' = \frac{\partial F}{\partial \eta} \tag{56}$$

$$Y_3 = F \tag{57}$$

$$F''' = [\beta(F'F' - 1) - FF''] \tag{58}$$

2) After solving the following differential equations, the following matrix is obtained:

$$\begin{bmatrix} Y_1^{n+1} \\ Y_2^{n+1} \\ Y_3^{n+1} \end{bmatrix} = \begin{bmatrix} Y_1^n + (\Delta n * ((Y_2^n - Y_6^n) - Y_3^n * Y_1^n)) \\ Y_2^n + \Delta n * Y_1^n \\ Y_3^n + \Delta n * Y_2^n \end{bmatrix} \tag{59}$$

Where Y^n is the previous values and Y^{n+1} are the forward values.

3.7 Falkner Skan Laminar Incompressible Flow Initial Conditions

This type of problem is solved as an Initial Condition or Initial Boundary value problem. Figure 2 shows the setup of the incompressible flow simulation, which is very similar to the compressible set up.

The initial boundary conditions near the wall are:

$$F'(0) = F(0) = 0 \tag{60}$$

$$F''(0) = Guess \tag{61}$$

The initial boundary conditions far from the wall:

$$F'(\infty) = 1 \tag{62}$$

3.8 Falkner Skan Incompressible Flow Simulation Algorithm

The Falkner-Skan incompressible equations are solved by using the point and shoot method which can be solved via a numerical derivative or a Runge Kutta method. In this work a numerical derivative was used to solve this equation.

Note: In the point and shoot method the value of $F''(0)$ is guessed until the $F'(\infty) = 1$ is reached.

The algorithm is as follows:
Inputs: U, ρ, μ, γ, L_y, h_y, β
$\upsilon = \mu/\rho$
Form η vector
Initial conditions: Y1=Guess, Y2=0, Y3=0
Loop start: for (i=1; length vector)
Previous Values Storage: Y10=Y1, Y20=Y2, Y30=Y3
$Y1 = (\Delta\eta * (\beta * Y20 * Y20 - Y30 * Y10)) + Y10$
$Y2 = Y20 + \Delta\eta * Y10$
$Y3 = Y30 + \Delta\eta * Y20$
Values storage (arrays): Y1(i)=Y1, Y2(i)=Y2, Y3(i)=Y3
Loop end

4. RESULTS AND CODE VALIDATION

4.1 Blasius Incompressible Solution Validation

Figure 3 shows the F' vs η theoretical values (red curve) for the Blasius incompressible flow solution ($\beta = 0$). A very good agreement with White [4] results can be observed. Also, it could be said that as η increases, F' also increases reaching asymptotically a unitary value around $\eta = 4$ (location of the boundary layer thickness).

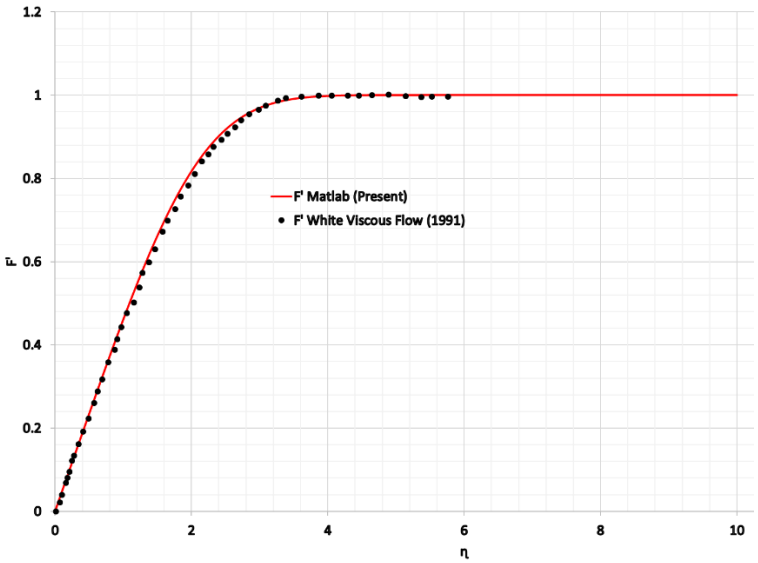

Fig. 3: F' vs η Blasius incompressible flow validation.

Figure 4 depicts F'' vs η theoretical values (red curve) for the Blasius incompressible flow solution. As observed in the figure, F'' obtained by our MATLAB code almost coincides with values from [4]. Also, it is important to mention that F'' starts at a guess value of 0.4696 and tends towards a zero value far from the wall, namely, in the inviscid region outside the boundary layer.

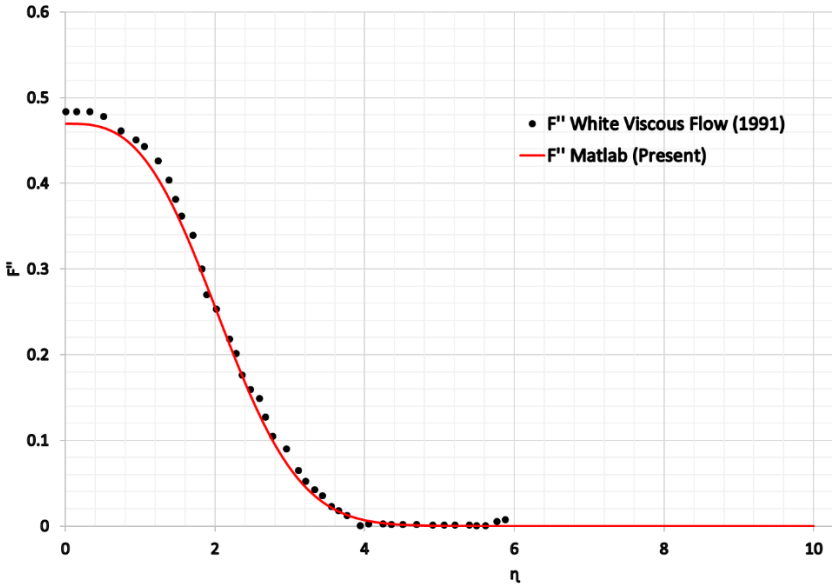

Fig. 4: *F*'' vs η Blasius incompressible flow validation.

4.2 Falkner Skan Incompressible Flow Validation for a Wedge flow of 27° and -16.2° degrees (β=0.3 and -0.18)

Figure 5 shows *F*' vs η theoretical values from the Viscous Flow book by White [4] (black symbols) and present MATLAB results (red) for the incompressible wedge flow at 27° (contraction or FPG case). As it can be seen in Figure 5, the MATLAB result highly coincide with the theoretical results showing a very good agreement. Since a Favorable Pressure Gradient (FPG) or acceleration is prescribed to the flow, it is observed a shrinking process of the boundary layer thickness. The ratio of the streamwise velocity (U) to the freestream velocity (U_e) (in other words, *F*') reaches a unitary value around $\eta \approx 3$.

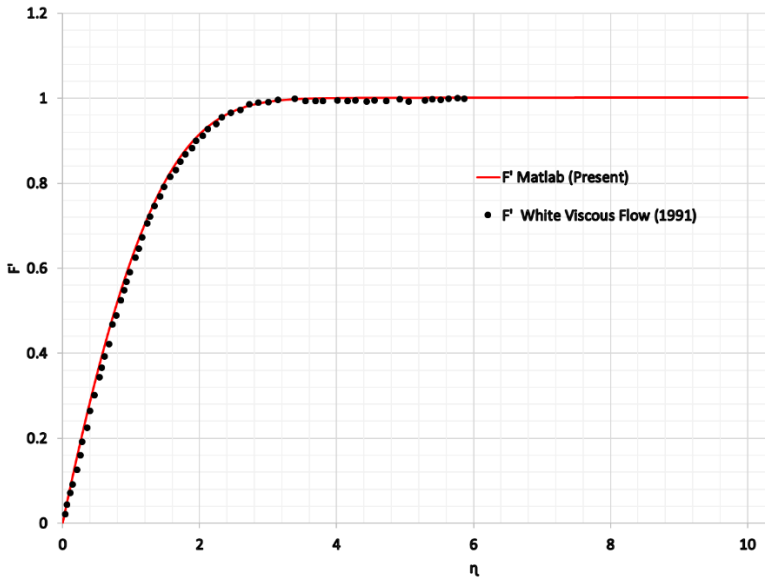

Fig. 5: *F*' vs η for the incompressible wedge at β=0.3 or FPG.

Similarly, Figure 6 shows the *F*'' vs η theoretical values from the Viscous Flow Book (black) and MATLAB (red) for the incompressible wedge flow solution of 27°. As observed in the figure, *F*'' values obtained with MATLAB almost overlap with results from [4]. The initial guess of *F*'' (0) was 0.77476, thus a significant increase of the wall shear stress with respect to the flat plate or Zero-Pressure Gradient (ZPG) case (in the order of 65%) is achieved by imposing a strong flow acceleration.

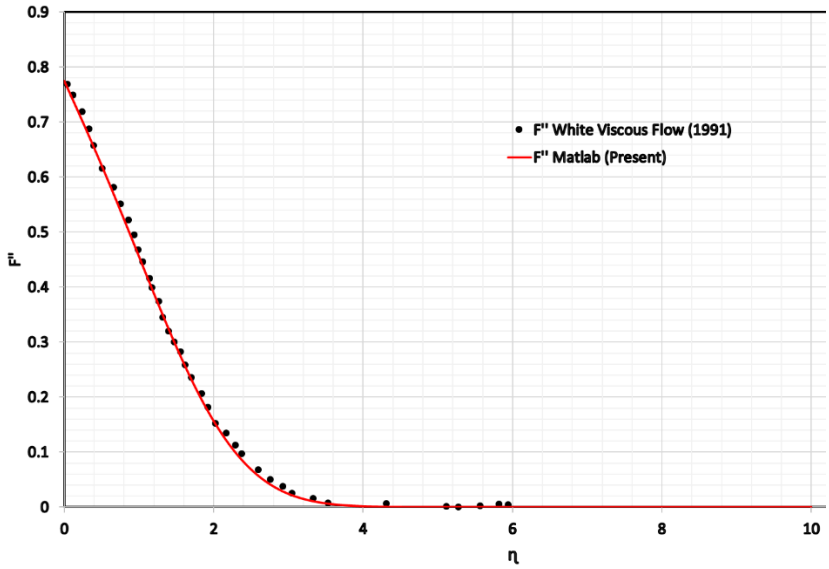

Fig 6: *F*'' vs η for incompressible wedge for β=0.3 or FPG.

Figure 7 shows *F*' vs η theoretical values from [4] (black symbols) and present MATLAB results (red) for the incompressible wedge flow solution of -16.2° (expansion or APG case). As it can be seen in the figure, present result seems to highly coincide with the theoretical results showing a very good agreement. Since an Adverse Pressure Gradient (APG) or acceleration is prescribed to the flow, it is observed a growing process of the boundary layer thickness. The ratio of the streamwise velocity (U) to the freestream velocity (U_e) (in other words, *F*') reaches a unitary value around $\eta \approx 5$.

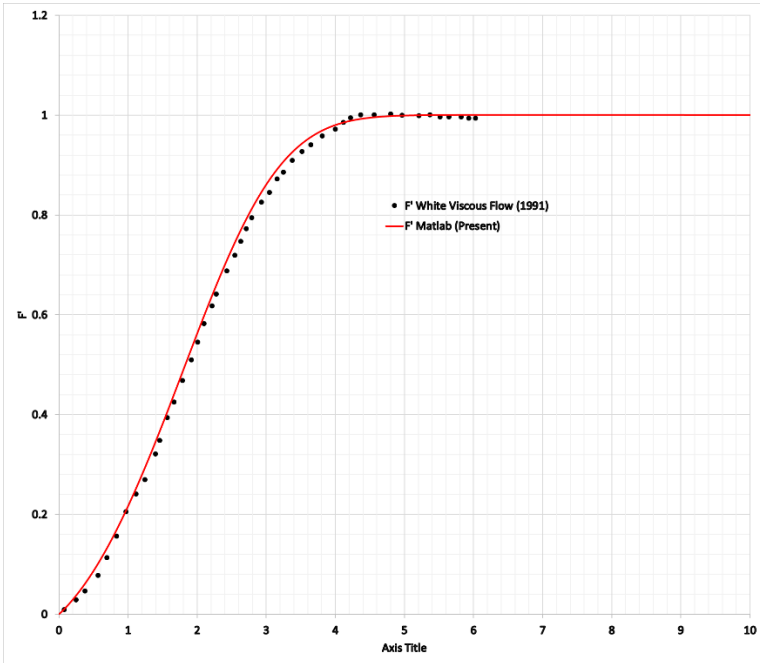

Fig. 7: F' vs η for incompressible wedge for β = -0.18

Figure 8 shows the *F*'' vs η theoretical for the incompressible wedge flow solution of -16.2° or β = -0.18. As observed in figure 8, the obtained *F*'' exhibits very good agreement with [4]. The initial guess of *F*'' (0) was 0.12864, thus a significant decrease of the wall shear stress (in the order of 70%) is achieved by imposing a strong flow acceleration. Notice that the value of β equal to -0.18 induces a very strong APG to the laminar boundary layer, which is prone to flow separation ($\beta_{critical}$ = -0.198838). Interestingly, the shear stress profile exhibits a local off-wall maximum at η = 1.8.

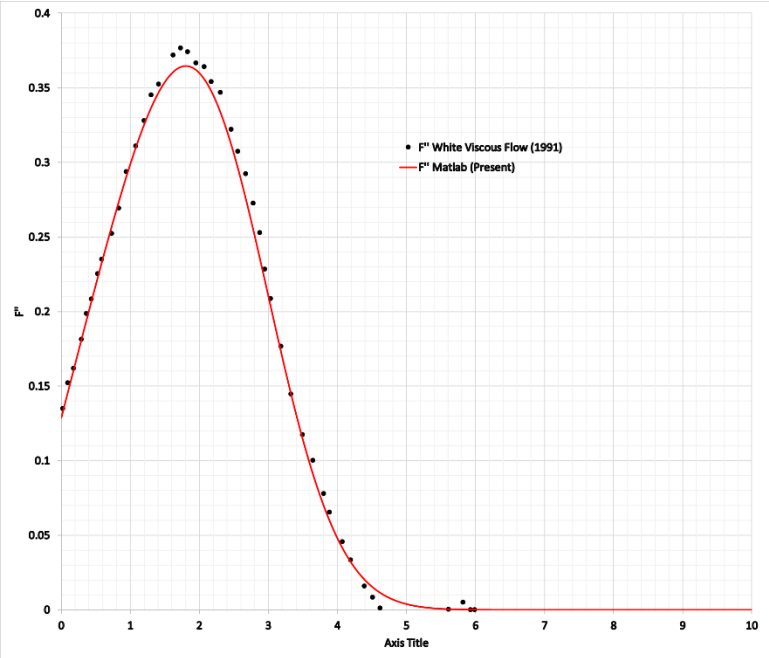

Fig. 8: *F*'' vs η for incompressible wedge for β = -0.18.

4.3 Falkner Skan Incompressible Flow for Different β Values

Figure 9 shows the *F*' distribution vs η for β of -0.18 (yellow), 0 (black), 0.3 (red) and 1 (green). The figure shows that as the flow acceleration increases (higher positive values of β) higher values of the streamwise velocity U are observed at the same wall normal coordinate η. The boundary layer thickness experiences a shrinking process in FPG flows. On the contrary, in APG flows (i.e., β = -0.18), the velocity profile *F*' tends to displace away from the wall, meaning that for APG the boundary layer thickness increases, due to the flow deceleration and boundary layer entrainment.

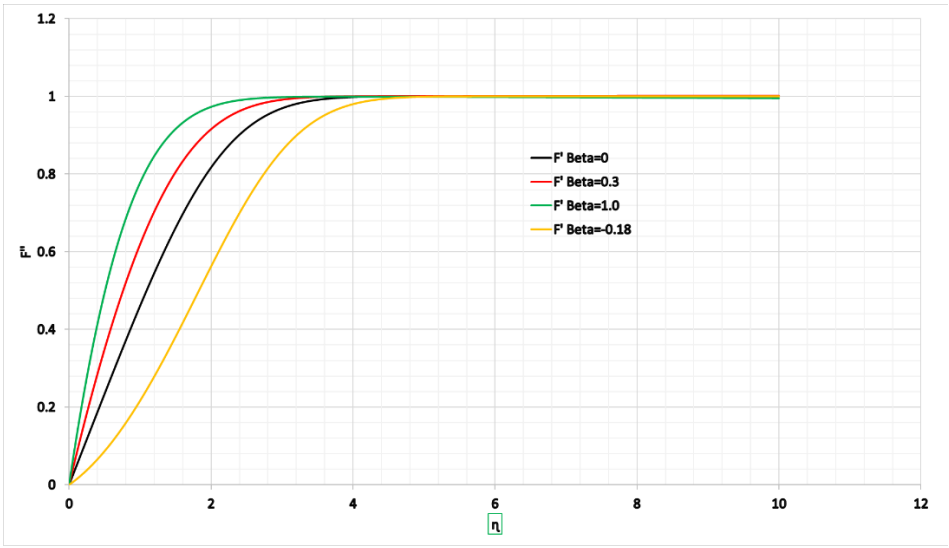

Fig. 9: *F*' vs η for Wedge Incompressible Flow for β of -0.18 (yellow), 0 (black), 0.3 (red) and 1.0 (green).

Figure 10 shows the *F*'' distribution as a function of η for β equal to -0.18 (yellow), 0 (black), 0.3 (red) and 1 (green). The figure shows that as β positively increases, wall shear stresses also increase, because in the

contraction the incompressible flow accelerates. As expected, F'' asymptotically decreases away from the wall, until reaching a zero-value at the edge of the boundary layer. Note that for the strong APG case or β = -0.18 significant values of the shear stress are observed in the outer region of the boundary layer, i.e. for η > 2.

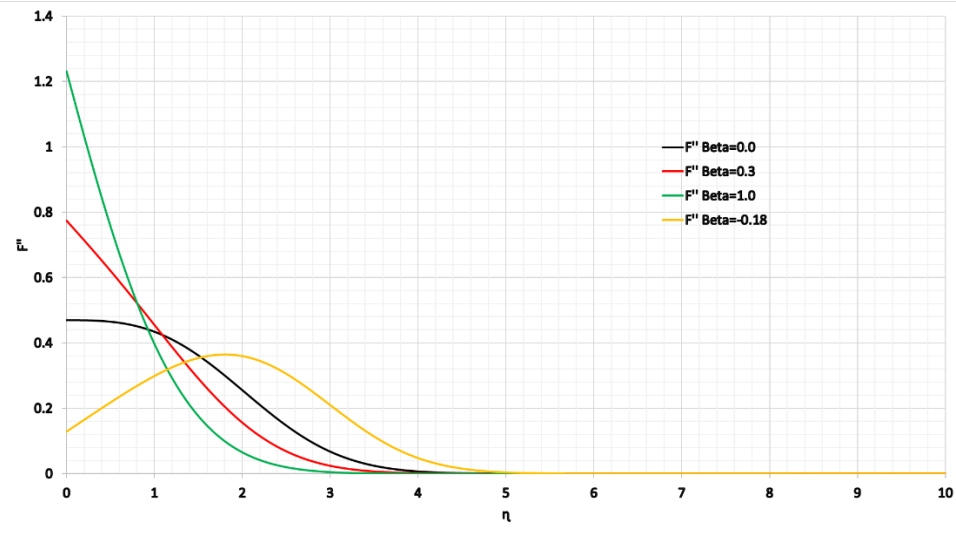

Fig. 10: F'' vs η for wedge incompressible flow.

4.4 Blasius Compressible and Incompressible Flow Comparison setting C = 1 and β = 0 Special Case

Figure 11 shows the F' vs η MATLAB Compressible (red) and White Viscous Flow Book [4] Incompressible (black) solution. It can be seen in the figure that the compressible and incompressible solutions are practically the same. This is because when C and β are set to 1 and 0 (ideal case), respectively, the compressible Blasius and Falkner-Skan solution are the same as the momentum conservation equation does not depend on the energy equation. This means that the momentum equation can be solved independently form the energy equation.

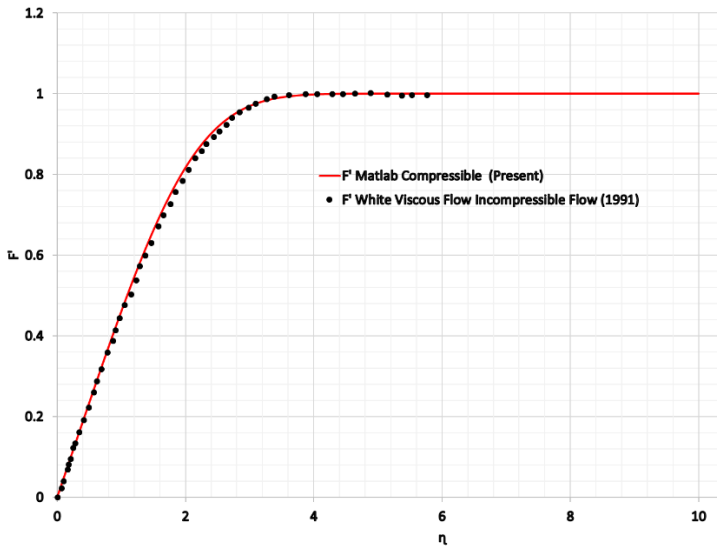

Fig. 11: F' vs η Blasius Incompressible and Compressible Solution Comparison.

Figure 12 shows the F'' vs η MATLAB Compressible (red) and White Viscous Flow Book Incompressible (black) solution. Again, it can be seen in the figure that the compressible and incompressible solutions nearly overlap.

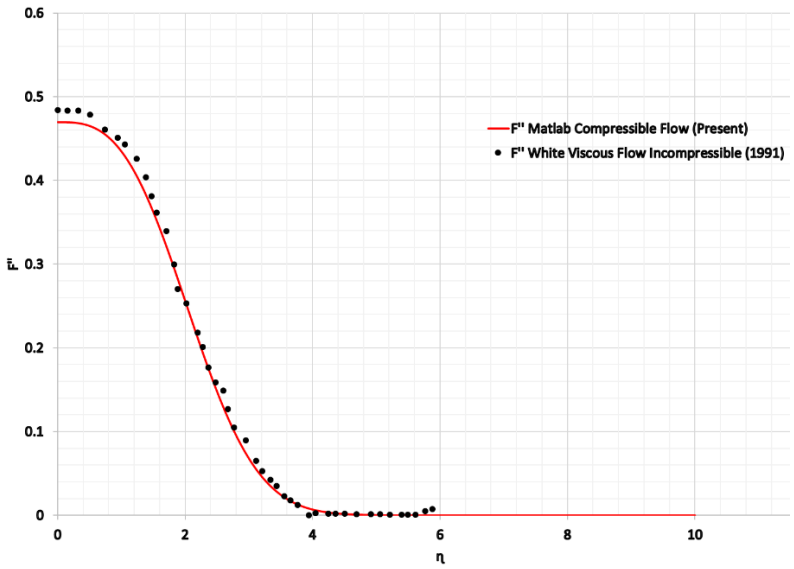

Fig. 12: *F*'' vs η Blasius Incompressible and Compressible Solution Comparison.

4.5 Blasius Solution for Various Mach Numbers, *P* = -0.24 and Pr = 0.71 for a flat plate

Figure 13 shows the *F*' distribution vs η for Mach of 2 (black), 4 (red), 6 (green), 8 (blue) and 10 (yellow). The figure shows that as the Mach number increases the curve tends to move leftward (closer to the wall) because it reaches a unitary value at an earlier η. Compressibility effects can be described as a local flow acceleration as the Mach number increases for the same value of η. Also, it is important to highlight that as the Mach number increases the boundary layer thickness significantly shrinks.

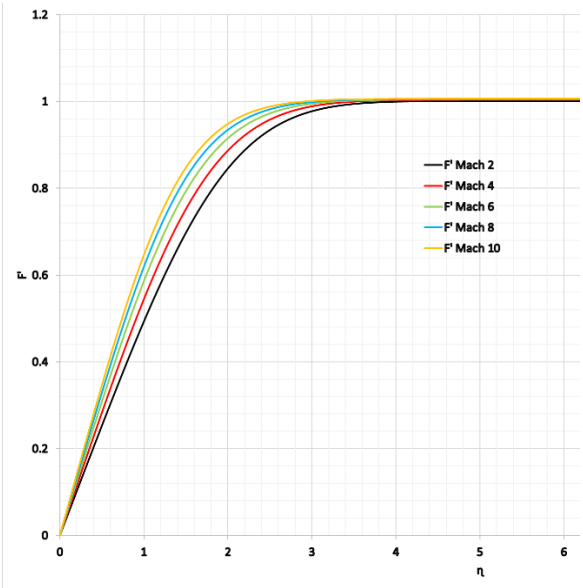

Fig. 13: *F*' vs η for Mach from 2 to 10.

Figure 14 shows the *F*'' vs. η distribution for different Mach numbers. The *F*'' values (proportional to the local shear stresses) exhibit a huge enhancement in hypersonic flows (i.e., Mach numbers higher than 5) and in the near wall region $\eta < 1.2$. Beyond that point of $\eta \approx 1.2$, all profiles at the different Mach numbers show a trend change: higher Mach number profiles depict lower values of the shear stress. This is consistent with the unitary value ($F' \rightarrow 1$ as $\eta \rightarrow \infty$) of the area enclosed by each curve.

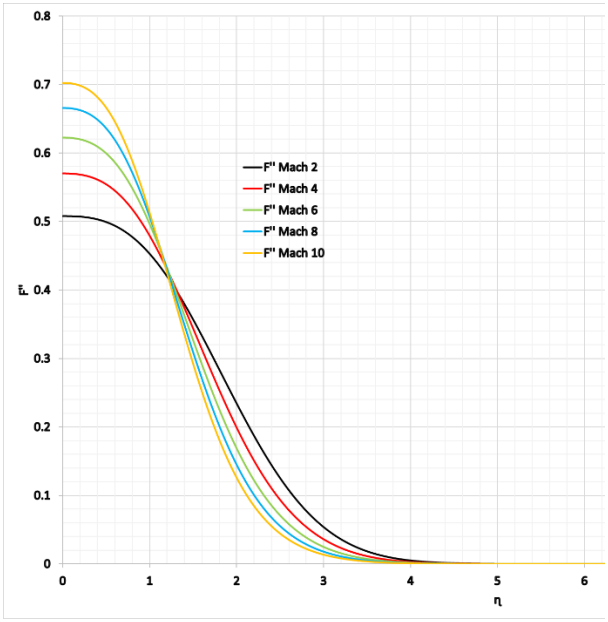

Fig. 14: F'' vs η for Mach from 2 to 10.

Figure 15 depicts the thermal distribution (g) for different Mach numbers under adiabatic wall condition. Contrary what occurred on the velocity field, the thermal boundary layer grows for the hypersonic regime. It also evident the significant heating of the fluid flow in the near wall region for Mach numbers larger than 6, e.g. at the hypersonic level. Local values of the temperature are up to 18 times larger than the freestream temperature.

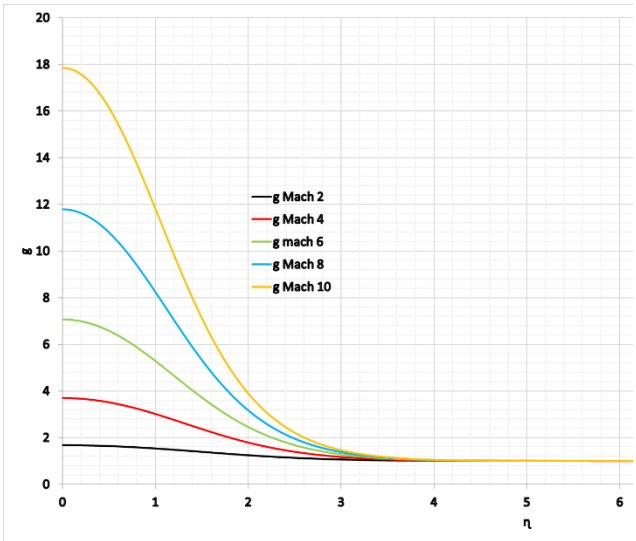

Fig. 15: g vs η for Mach numbers from 2 to 10.

6. CONCLUSIONS

The algorithm developed for Falkner-Skan incompressible and compressible laminar flows was successfully validated. The Blasius special case for $C = 1$ and $\beta = 0$ for compressible flow yielded very similar results to the incompressible counterpart solution since the momentum equation is decoupled from the energy equation. Compressibility effects have been identified as a local increase of the streamwise velocity U as the Mach number increases for the same vertical coordinate. While the hydrodynamic boundary layer exhibits a strong shrinking process in the hypersonic regime, the thermal boundary layer grows. Furthermore, the thermal load strikingly augments beyond Mach numbers of 6 and adiabatic wall conditions.

ACKNOWLEDGMENT

This material is based upon work supported by the Air Force Office of Scientific Research under award number FA9550-17-1-0051 and Program Officer Dr. Ivett Leyva.

NOMENCLATURE

ξ	dimensionless variable (-)
ρ_e	Density at wedge edge (kg/m^3)
U_e	Velocity at wedge edge (m/s)
μ_e	Dynamic viscosity at the wedge edge (Pa/s)
η	dimensionless variable (-)
t	time (s)
h	Enthalpy (W/kg)
P_e	Pressure at Wedge Edge (Pa)
P	Local Pressure (Pa)
u	Local velocity x (m/s)
v	Local velocity y (m/s)
ρ	Local Density (kg/m^3)
ρ_∞	Free stream Density (kg/m^3)
x	Distance x direction (m)
y	Distance y direction (m)
C	Dimensionless ration between density and viscosity and edge density and viscosity (-)
F''	Dimensionless Shear Parameter (-)
F'	Dimensionless Velocity Parameter (-)
F	Dimensionless Free Stream Parameter (-)
g'	Dimensionless Heat Flux (-)
g	Dimensionless Temperature ratio parameter (-)
Pr	Prandlt Number (-)
Mach	Mach number (-)
β	Pressure Gradient (-)
Cf_x	Skin friction coefficient (-)
τ_w	Wall Shear Stress (Pa)
θ	Wedge Angle (Radians)
m	Power Law Parameter (-)
a	Constant (-)

REFERENCES

[1] "Clay Mathematics Institute," [Online]. Available: https://www.claymath.org/millennium-problems/navier%E2%80%93stokes-equation.

[2] Yunnus. A. Cengel and Jhon M. Cimbala, Fluid Mechanichs Fundamentals and Applications, New York: McGraw-Hill, 2014.

[3] I. Tani, "History of Boundary Layer Theory. Annual Review of Fluid Mechanics," *Annual Review of Fluid Mechanics,* vol. 9, pp. 87-111, (2003).

[4] Frank M. White, Viscous Fluid Flow, New York: MacGraw-Hill, 1991.

[5] Y. Cho and A. Aessopos, "Similarity transformation methods in the analysis of the two dimensional steady compressible laminar boundary layer," *Mechanical Engineering, Massachusetts Institute of Technology* , 2004 .

[6] N. Curle, THE LAMINAR BOUNDARY LAYER EQUATIONS, New York: DOVER, Publications Inc., 2017.

[7] H. Tennekes and J. M. Lumley, A FIRST COURSE IN TURBULENCE, MASSACHUSETS: MIT PRESS, 1972.

[8] [Online]. Available: http://brennen.caltech.edu/fluidbook/basicfluiddynamics/turbulence/lawofthewall.pdf.

[9] M. Xenos, E. Tzirtzilakis, N. Kafoussias, "Methods of optimizing separation of compressible turbulent boundary-layer over," *International Journal of Heat and Mass Transfer,* p. 488–496.

[10] M. Xenos and I. Pop, "Radiation effect on the turbulent compressible boundary layer flow with adverse pressure gradient," *Applied Mathematics and Computation,* p. 153–164, 2016.

[11] T. Cebeci and A. M. O. Smith, ANALYSIS OF TURBULEN BOUNDARY LAYERS, New York: Academic Press, 1974.

[12] B. Baldwin and H. Lomax, "Thin-layer approximation and algebraic model for separated turbulent flows," *AIAA* , vol. Proceedings of the Sixteenth Aerospace Sciences Meeting, p. Paper. 78–205., 1978 .

[13] D. KNIGHT, H. YAN and Z. A. ZHELTOVODOV, "LARGE EDDY SIMULATION OF SUPERSONIC TURBULENT FLOW IN EXPANSION-COMPRESSION CORNER," *Defense Technical Information Center Compilation Part Notice ADP013634.*

[14] M. Holden, A. Havener and C. Lee, "Shock Wave/Turbulent Boundary Layer Interaction in High-Reynolds-Numbers Hypersonic FLows," *Anual Report USAF,* 1987.

[15] S. Xu and P. M. Martin, "Assesment of inflow boundary conditions for compressible turbulent boundary layers,"," *AIP Physics of Fluids,* vol. vol. 16, no. no. 7, pp. pp. 2623-2639, 2004.

[16] E. Sanger and J. Bredt, "A ROCKET DRIVE FOR LONG RANGE BOMBERS," *Deutsche Luftfahrtforschung* , 1944 .

[17] R. H. Speier, N. George, C. A. Lee and R. M. Moore, "Hypersonic Missile Nonproliferation Hindering the Spread of a New Class of Weapons," *RAND Corporation,* 2017 .

[18] T. A. Heppenheimer, "Facing the Heat Barrier: A History of Hypersonics," *The NASA History Series,* 2007 .

[19] Frank M. White, Viscous FLow, McGraw Hill, 1991.